DOI: 10.19884/j.1672-5220.202401001

Corneal Topographic Restoration Imaging Based on Placido Disc

WAN Xuanrun[1], WANG Chaoxing[1], HU Jun[2,3], JIANG Jian[4,5*], LI Kangmei[1*]
1. College of Mechanical Engineering, Donghua University, Shanghai 201620, China
2. Institute of Artificial Intelligence, Donghua University, Shanghai 201620, China
3. Shanghai Industrial Big Data Engineering Technology Research Center, Shanghai 201620, China
4. Eye Hospital, Wenzhou Medical University, Wenzhou 325000, China
5. Zhejiang Eye Hospital, Wenzhou 325000, China

Abstract: Corneal topography serves as an essential reference for diagnostic treatment in ophthalmology. Accurate corneal topography is crucial for clinical practice. In this study, the refractive power calculation was performed based on the initial corneal information collected using the Placido disc. A corneal point cloud model was established in polar coordinates, and an interpolation algorithm was proposed to fill missing points of the local bicubic B-spline by searching control points in the self-defined interpolation matrix. The grid interpolation of the point cloud information and the smooth imaging of the final topographic map were achieved by Delaunay triangulation and Gaussian kernel function smoothing. Experiment results show that the proposed interpolation algorithm has higher accuracy than previous algorithms. The mean absolute error between the measured diopter of the original detection and the reconstructed is less than 0.300 D, indicating that this algorithm is feasible.

Keywords: corneal topography; Placido disc; point cloud model; bicubic B-spline; Gaussian kernel function
CLC number: R778 **Document code**: A
Article ID: 1672-5220(2025)02-0204-09

Open Science Identity (OSID)

0 Introduction

The cornea is the most important refractive physiological structure before light enters the retina, and its susceptibility to deformation is a significant factor contributing to ocular diseases such as myopia and keratoconus[1-3]. Corneal topography provides a quantitative, color-coded representation of corneal surface refraction and other information displayed in layers. It reflects the true three-dimensional shape of the cornea and serves as an essential reference in the field of ophthalmology for keratomileusis fitting, pre-operative and post-operative keratomileusis examinations and other ophthalmic treatments[4-6]. The Placido disc is an important instrument for collecting information from various points on the cornea[7-8]. By processing the reflected light from the corneal surface, it is possible to obtain preliminary information about the corneal surface, which is the basis for computerized corneal topography generation.

In the field of computerized corneal topography, Xu et al.[9] used ray inverse tracking with edge detection to extract subpixel data from the Placido disc ring for corneal topography imaging. However, this method relies on the assumption of an ellipsoidal corneal surface, resulting in a correction to the standard ellipsoidal surface. Zhou et al.[10] proposed an improved Shepard corneal surface interpolation method. It exhibited slightly poor accuracy due to the limitaion of the principles of the interpolation algorithm, and it was computationally intensive and time-consuming when dealing with a large number of missing points. Florindo et al.[11] performed image boundary segmentation and reconstruction based on the Mumford-Shah algorithm. However, the whole process was cumbersome and complicated, which made it difficult to meet the practical application requirements.

The point cloud model is one of the best ways to describe the corneal surface. In response to the challenges posed by limited accuracy and computational complexity in the previously mentioned restoration algorithm, this study introduces a corneal surface missing-point filling algorithm based on bicubic B-spline. Building on the established polar coordinate corneal point cloud model, the algorithm employs Delaunay triangulation for mesh interpolation and incorporates a Gaussian kernel function for data point convolution smoothing. This approach is expected to achieve the high-precision reconstruction of computer-generated corneal topographic images.

Received date: 2024-01-05
Foundation item: Shanghai Science and Technology Program, China (No. 20DZ2251400)
* Correspondence should be addressed to JIANG Jian, email: jiangjianwmu@wmu.edu.cn; LI Kangmei, email: lkm718@126.com
Citation: WAN X R, WANG C X, HU J, et al. Corneal topographic restoration imaging based on Placido disc[J]. *Journal of Donghua University (English Edition)*, 2025, 42(2): 204-212.

1 Acquisition and Transformation of Placido Disk Detection Images

1.1 Image acquisition of Placido disc

The Placido disc is composed of a series of black and white concentric rings centered on the optic axis to detect the cornea of the instrument[12], as shown in Fig. 1. For the Placido disc image acquisition to the imaging process, the acquisition system consists of the Placido disc, the projector and the charge-coupled device (CCD) image acquisition system. Light is transmitted through the white concentric rings projected onto the corneal surface from the center to the peripheral region in turn, the entire cornea light is reflected to the CCD, and the individual pixels reflected from each point are converted into digital signals by the CCD. At the same time, the imaging digital signal is analyzed and processed by the image acquisition system to calculate the characteristic information of each collected point, and the final corneal imaging is processed by the computer.

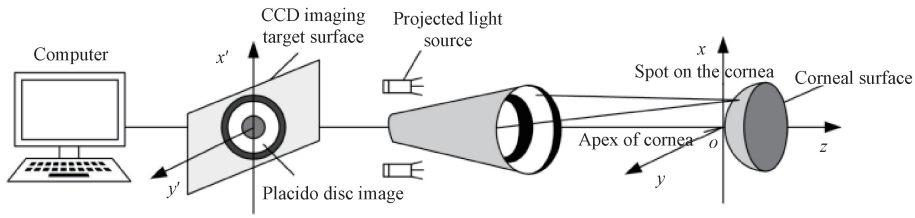

Fig. 1 Placido disc image acquisition to imaging procedure

1.2 Diopter conversion

The corneal information collected as described above is processed mainly as the curvature information of corneal points. The diopter reflects the ability of the eye to refract light and is one of the most important indicators for physicians in clinical practice, as well as the main corneal diagnostic outcome data used to present corneal topography.

The axial diopter provides a good representation of the overall shape of the cornea, and it is generally used to outline the overall shape of the corneal surface[13]. The schematic diagram of the axial refraction is shown in Fig. 2. The corneal vertex is used as the reference point, and the center of all light is placed in the axial direction of the diopter. In Fig. 2, A represents a point on the cornea, and its coordinates are (x_A, y_A). The dashed line indicates the normal direction at point A and intersects the coordinate axis at A'. The distance between point A and A' is denoted as r_A and the slope angle is represented by α.

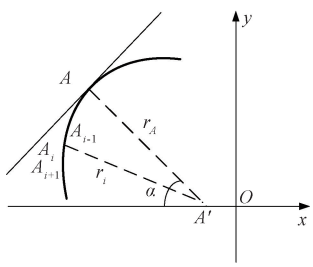

Fig. 2 Schematic diagram of axial refraction

r_A can be depicted as follows:

$$r_A = \frac{y_A}{\sin \alpha}. \tag{1}$$

Thus, the axial diopter D_A can be obtained from the relationship between the diopter and curvature transformation:

$$D_A = \frac{n-1}{r_A}, \tag{2}$$

where n is the corneal refractive index and $n = 1.337\ 5$.

An instantaneous diopter is used to characterize the features of the corneal surface and corresponds to the local radius of the cornea curvature[14]. Considering the aspheric nature of the cornea, the instantaneous diopter can better describe the true curvature radius of the cornea. Assuming that three adjacent points on the same corneal meridian can be approximated as an arc of a circle, each point is the same distance from the center of the circle. If the coordinates of the three adjacent points on the same meridian are (x_{i-1}, y_{i-1}), (x_i, y_i) and (x_{i+1}, y_{i+1}), the center of the arc is represented by the coordinates (x_A, y_A), and the radius of curvature is denoted as r_i, the following equations can be set out:

$$\begin{cases} (x_{i-1}-x_A)^2+(y_{i-1}-y_A)^2 = r_i^2, \\ (x_i-x_A)^2+(y_i-y_A)^2 = r_i^2, \\ (x_{i+1}-x_A)^2+(y_{i+1}-y_A)^2 = r_i^2. \end{cases} \tag{3}$$

The relationship between (x_A, y_A) and r_i can be found according to Eq. (3):

$$x_A = \frac{(x_i^2+y_i^2)(y_{i-1}-y_{i+1})+(x_{i-1}^2+y_{i-1}^2)(y_{i+1}-y_i)+(x_{i+1}^2+y_{i+1}^2)(y_i-y_{i-1})}{2[(x_i-x_{i-1})(y_i-y_{i+1})-(x_i-x_{i+1})(y_i-y_{i-1})]}, \tag{4}$$

$$y_A = \frac{[\,y_{i-1}+y_i+(x_i+x_{i-1}-2x_A)(x_i-x_{i-1})\,]}{2(y_i-y_{i-1})}, \quad (5)$$

$$r_i = \sqrt{(x_i-x_A)^2+(y_i-y_A)^2}. \quad (6)$$

The instantaneous diopter can be obtained from the relationship between the diopter and curvature transformation:

$$D_i = \frac{n-1}{r_i} = \frac{0.337\,5}{r_i}. \quad (7)$$

2 Corneal Point Cloud Model Analysis Imaging

2.1 Polarization of coordinates

Due to the large number of corneal data points collected, it is difficult to determine the coordinates for the establishment of the point cloud model in a rectangular coordinate system. Given the characteristics of the images acquired by the Placido disc, the point cloud coordinate system is established in polar coordinates in this study. This can be seen in Fig. 3 (a) which represents a schematic diagram of the Placido disc projected onto the human eye. Figure 3 (b) shows a schematic of the resulting polar coordinate system, where L is the distance from the point on the image to the center of the cornea, and θ is the angle of the point away from the polar axis.

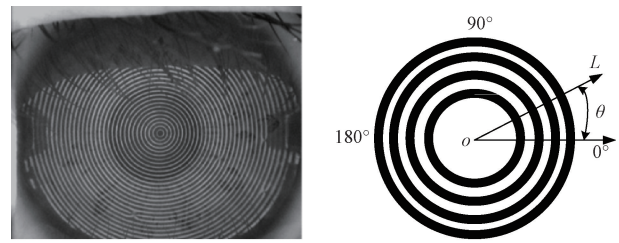

(a) (b)

Fig. 3 Schematic of resulting polar coordinate system: (a) Placido disc projected onto human eye; (b) polar coordinate system

2.2 Missing-point filling based on bicubic B-splines

Ideally, the Placido disc can collect all the reflected corneal data points. However, eyelash blockage and other reasons cause a large number of missing data points during the actual collection process. The missing data points lead to a pronounced discontinuity in the point cloud model, as shown in Fig. 4, which affects the subsequent corneal three-dimensional imaging thereby affecting the accuracy of the topographic map. The idea of B-splines is to use a flexible strip that is tough enough to pass through the selected interpolated data points under stresses to form a smooth curve or surface, thus enabling the interpolation of unknown points[15-16]. In this study, the missing data points are interpolated and filled by fitting a local bicubic B-spline surface.

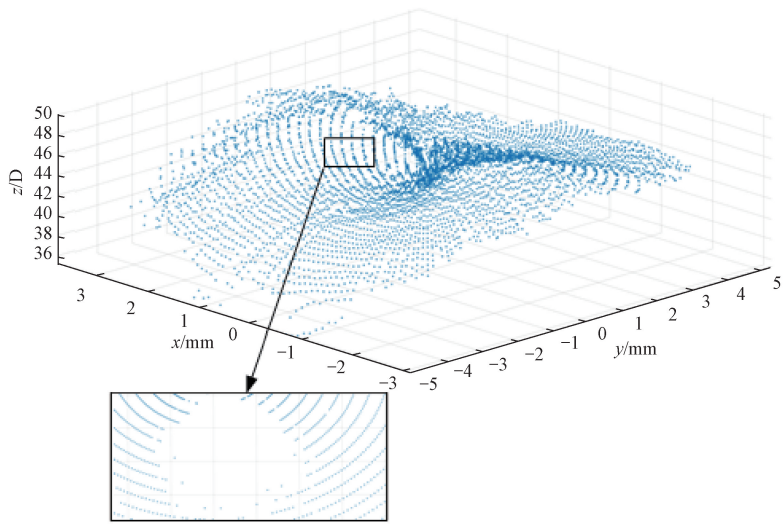

Fig. 4 Schematic of missing points in point cloud

Let the set of discrete points in three-dimensional space be $T=\{(x, y, D_i)\}$ and T is approximated by $m \times n$ bicubic B-spline surface slices. These $m \times n$ bicubic B-spline surface patches are represented by the control mesh volume $F_{(i+p)(j+l)}$, which is composed of the surrounding 16 control points. The resulting bicubic B-spline interpolation function is

$$F(x, y) = \sum_{p=0}^{3}\sum_{l=0}^{3} B_p(s)B_l(\alpha)F_{(i+p)(j+l)}, \quad (8)$$

where the double summation $\sum_{p=0}^{3}\sum_{l=0}^{3}$ iterates over the 4×4 control points and computes the weighted contribution of each; B_p and B_l are the B-spline basis functions that determine the influence of the control points in the x- and y-directions; s and α are normalized parameters indicating the relative position of x and y within the grid cell; $F_{(i+p)(j+l)}$ represents the known function values at the control grid points $(i+p, j+l)$, and contributes to the

value of $F(x, y)$. The bicubic B-spline interpolation formula represents the function value at position (x, y). Equation (8) calculates the value at any point (x, y) by performing a weighted average of these control points and basis functions, thus achieving bicubic B-spline interpolation. The basis function of the bicubic B-spline for this study is

$$\begin{cases} B_0(u) = (1 - 3u + 3u^2 - u^3)/6, \\ B_1(u) = (4 - 6u^2 + 3u^3)/6, \\ B_2(u) = (1 + 3u + 3u^2 - 3u^3)/6, \\ B_3(u) = u^3/6, \end{cases} \tag{9}$$

where u represents the parameter value and defines the position of the current calculated point in the node interval. Specifically, u is a normalized parameter that typically takes on values in a node interval, typically in the range $[0, 1]$. As a point moves along a curve from one node to another, u represents the relative position of the point on the curve within this interval between nodes.

The problem of finding the partitioned small mesh surface is to find the interpolation problem of bicubic B-splines. In the case of fully considering the selection of influence points, this study established a 5 × 5 interpolation matrix to reduce the program complexity and calculation amount. The closest 16 points surrounding the point to be interpolated (that is, the sixteen points with the smallest radial distance from the point to be interpolated) are selected as the control points that affect the interpolated data. As shown in Fig. 5, the red circle points are the points to be interpolated; the triangles are the sample points; B_{pl} represents the sampling point involved in bicubic B-spline interpolation. Due to the lack of sample points, there may be blank points in the interpolation matrix. When searching for the control points, the radial distance between the points existing in the 5 × 5 interpolation matrix and the points to be interpolated is calculated, and the grid is generated by using the 16 control points. The 16 control points are substituted into the basis function Eq. (9) in turn to calculate their respective basis function values. The calculated basis function values of each point and the data value of each control point are substituted into Eq. (8) to obtain $F(x, y)$ to be interpolated.

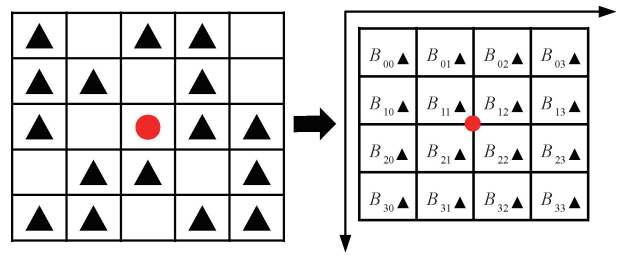

Fig. 5 Schematic diagram of bicubic B-spline interpolation implementation

2.3 Corneal topography

Gridding is the process of dividing the discrete point cloud data into a grid of regular features. The maximum number of point clouds actually processed in this study is 300 × 32 = 9 600, here the plot data domain is divided into 200 parts by polar coordinates, and the radian of each angle is $\pi/200$. The data domain is divided into a grid of 200 × 200 = 40 000, and the known point cloud data are converted into grid point data. Delaunay triangular dissection is a special kind of triangle dissection. If there are two points in the set of points V where the outer circle of the two points does not contain any other points in V, then the line connecting these two points is the Delaunay edge[17-18]. In this study, the entire point cloud collection is subjected to a two-dimensional Delaunay triangulation process to create a Delaunay trianglar mesh, as depicted in Fig. 6 for the local region generated in this study. The red points denote the centers of the Delaunay triangles, and the grid points located within the Delaunay triangles (the Voronoi diagram region) are interpolated into the mesh using a natural neighborhood approach. The mesh is interpolated, and the values are replaced by 0 if the mesh is not within the Voronoi diagram region.

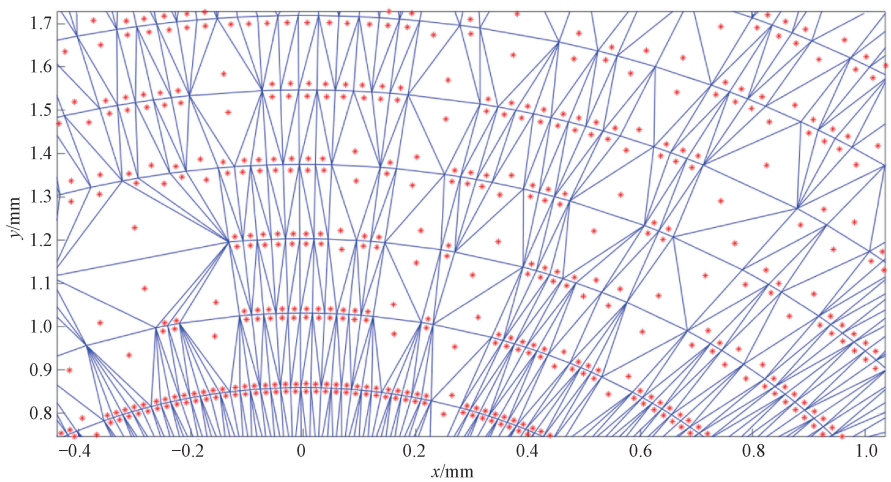

Fig. 6 Localized areas of Delaunay triangular mesh

The initial modeling and imaging of the cornea's three-dimensional image and topography are shown in Figs. 7(a) and 7(b). In Fig. 7, warm colors correspond to higher values in the diopter, indicating relatively steep areas on the cornea; cool colors represent lower values in the diopter, denoting relatively flat areas; D is the unit of diopter, and 1 D = 1 m^{-1}. A clear discontinuity in the graphical features of the topography requires image smoothing. Gaussian kernel function is an effective tool for image smoothing, and the smoothing based on the two-dimensional Gaussian function[19] is used in this study. The expression of the two-dimensional Gaussian function is

$$G(x,y)=\frac{1}{2\pi\sigma^2}\exp\left[\frac{-(x^2+y^2)}{2\sigma^2}\right], \tag{10}$$

where σ is the standard deviation and determines the smoothing degree of the image. When σ is high, the more dispersed the distribution of weights, the smaller the difference between the weights of each part, and thus the transition is more rounded; when σ is low, the more centralized the distribution of weights, the larger the difference between the weights of each part, and thus the transition is rougher. Given the magnitude of the local influence, σ is set as five to smooth the initial three-dimensional modeled corneal image and complete the final corneal topography image (Fig. 7(c)).

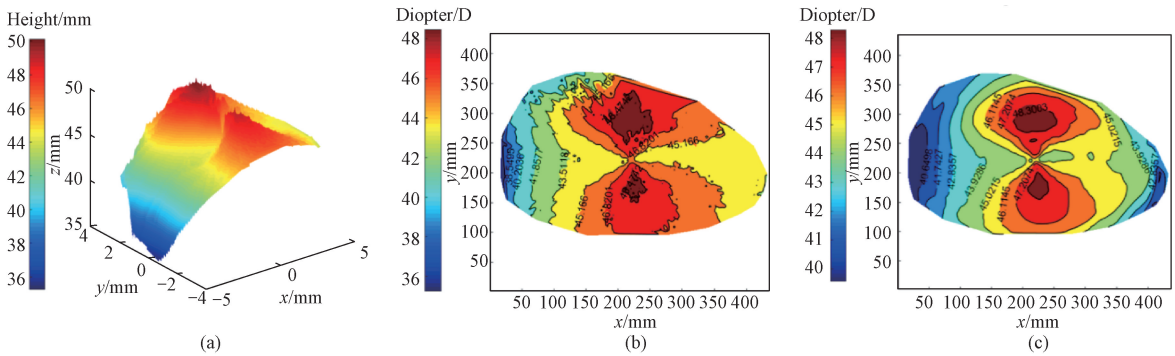

Fig. 7 Modelling of corneal: (a) initial modeling of corneal three-dimensional image; (b) initial modeling of corneal topography; (c) final modeling of corneal topography

3 Experiments and Analyses

3.1 Analysis of missing-point filling algorithms

To verify the effectiveness of the missing-point filling algorithm proposed in this study, the interpolation algorithm based on bicubic B-splines is used to interpolate the known 3 000-point cloud data, and the interpolated results are compared with the inverse distance interpolation algorithm proposed in Ref. [20] as well as the true value.

Due to the huge amount of experimental data, this study only shows the interpolation results of part of the point cloud data, as shown in Table 1. For 3 000-point cloud data, the relative error distribution of the interpolation methods is shown in Fig. 8.

Table 1 Comparison of 3 000-point cloud data and interpolated data

Coordinate value		Diopter/D		
x/mm	y/mm	True value	Bicubic B-spline interpolation	Inverse distance-weighted interpolation
0.153 8	0.076 7	43.91	43.83	44.58
−4.462 6	0.234 7	39.78	39.88	40.34
−3.207 7	1.235 8	42.52	42.71	42.09
−1.778 1	0.642 5	44.34	44.23	44.43
5.298 7	−0.558 8	37.21	37.47	37.43
⋮	⋮	⋮	⋮	⋮
2.109 3	−0.737 2	42.25	42.09	41.69
1.298 4	−1.126 2	47.54	47.53	48.25
−2.459 4	0.773 5	43.78	43.59	43.41
−0.104 9	−0.136 1	45.63	45.27	45.72
−3.952 9	−0.041 5	41.34	41.09	41.93

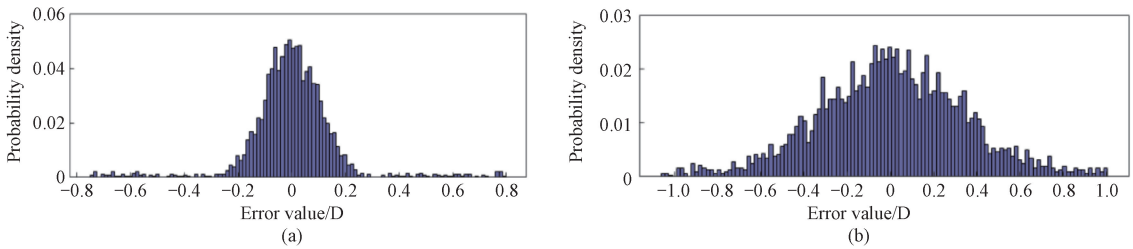

Fig. 8 Histogram of error distribution of interpolation method: (a) bicubic B-spline interpolation error distribution; (b) inverse distance-weighted interpolation error distribution

From the data and the histograms, it can be concluded that the bicubic B-spline interpolation method is more accurate, with a tighter error distribution around zero and generally smaller deviations from the true values. The inverse distance interpolation method shows larger errors and a broader error distribution, which may make it less reliable for precise applications.

The specific evaluation metrics of the error distribution histograms are shown in Table 2, and the three error evaluation metrics corresponding to the local bicubic B-spline interpolation method proposed are smaller than those corresponding to the inverse distance-weighted interpolation method, which suggests that this algorithm is more suitable for the corneal point cloud missing-point filling interpolation.

Table 2 Statistical analysis of interpolated data by different interpolation methods

Interpolation method	Mean absolute error/D	Mean squared error/D^2	Standard deviation/D
Bicubic B-spline interpolation	0.109	0.002	0.173
Inverse distance-weighted interpolation	0.267	0.005	0.341

3.2 Corneal topography imaging analysis

In order to verify the feasibility of the restoration algorithm in this study, the accuracy of the corneal topographies recovered was compared and analyzed to determine the superiority of the algorithm. The results from the Medmont (E300U, Australia) corneal topography restoration software were chosen as the reference for comparison in this study. The same patient was selected for examination, and the initial data from the Placido disc examination were collected. Subsequently, the axial and tangential corneal maps of the patients' recovered corneas were compared respectively. The corneal data on the 0°, 90°, 180° and 270° half meridian of the recovered topographic maps, axial maps, and tangential maps were selected and compared with the original corneal data acquired by the Placido disc. The restoration results of axial maps evaluated along distinct meridians are presented in Fig. 9 and Table 3. The restoration results of tangent plots are presented in Fig. 10 and Table 4.

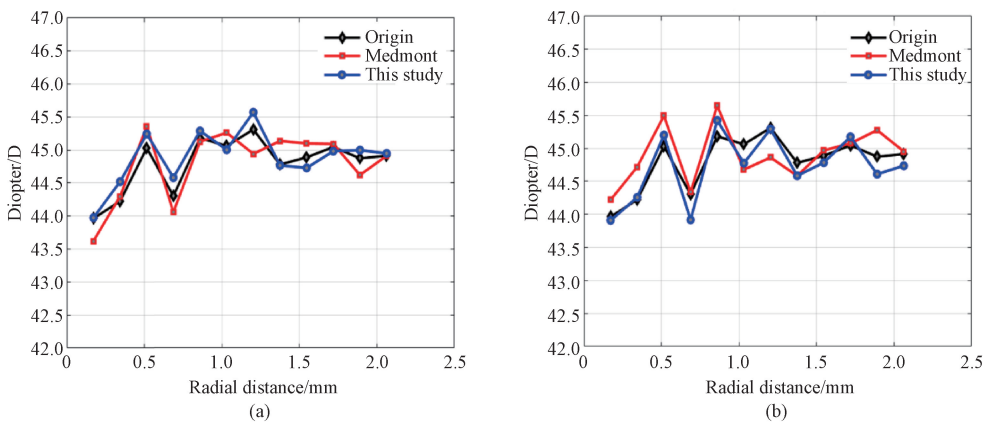

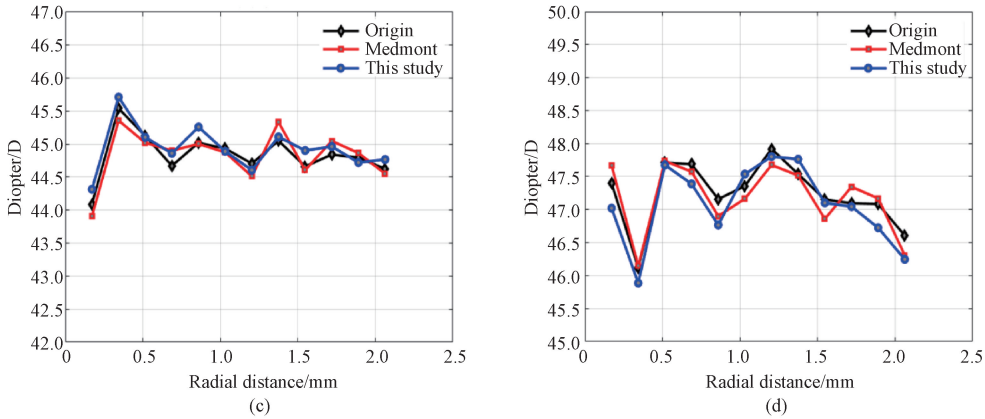

Fig. 9 Comparison of axial map along distinct meridians: (a) 0°; (b) 90°; (c) 180°; (d) 270°

Table 3 Difference between each meridian and original data in axial map

Method	Mean absolute error/D			
	0°	90°	180°	270°
Medmont	0. 207	0. 138	0. 173	0. 275
This study	0. 135	0. 135	0. 223	0. 172

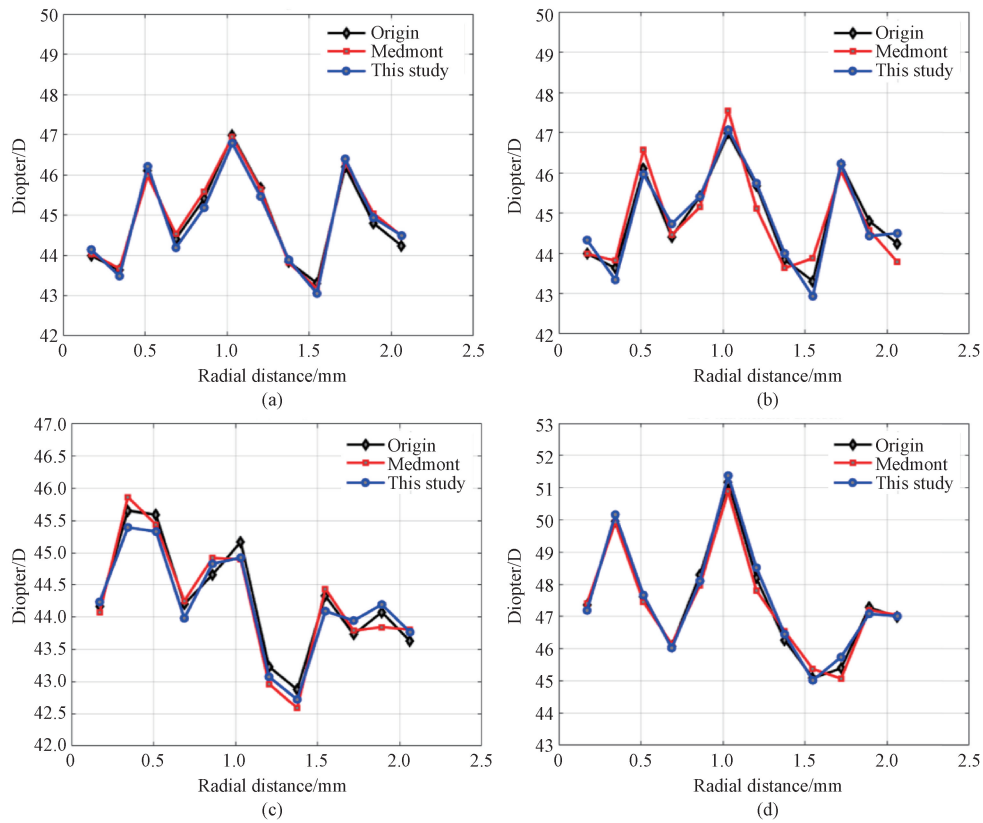

Fig. 10 Comparison of tangent plot along distinct meridians: (a) 0°; (b) 90°; (c) 180°; (d) 270°

Table 4 Difference between each meridian and original data in tangent plot

Method	Mean absolute error/D			
	0°	90°	180°	270°
Medmont	0. 211	0. 181	0. 194	0. 310
This study	0. 178	0. 187	0. 168	0. 202

The computerized corneal topography restoration algorithm proposed in this study shows comparable performance to the method used in the Medmont corneal topography restoration software. The error between the restored topography and the original corneal examination data remains relatively stable. Additionally, the mean absolute error is generally less than 0.300 D, which is within the permissible error range. This indicates that the method proposed in this study is feasible.

4 Conclusions

In this study, a corneal topography restoration method based on initial information from Placido disc detection is proposed. The problem of difficult coordinate determination during corneal point cloud modeling is solved by using polar coordinate modeling. An algorithm based on filling missing points in the bicubic B-spline point cloud is proposed. The algorithm automatically searches for control points within the established interpolation matrix, which reduces the complexity of procedure implementation and achieves a higher accuracy compared with the widely used inverse distance-weighted interpolation. The application of the Gaussian kernel function addresses the issue of image feature discontinuity and completes the smoothing of topographic maps. The entire reconstruction process demonstrates a high level of accuracy and feasibility, with minimal discrepancies between the reconstructed results and the original corneal examination data. The mean absolute error remains below 0.300 D, thereby satisfying the medical requirements.

References

[1] ESPANA E M, BIRK D E. Composition, structure and function of the corneal stroma[J]. *Experimental Eye Research*, 2020, 198: 108137.

[2] MOBARAKI M, ABBASI R, VANDCHALI S O, et al. Corneal repair and regeneration: current concepts and future directions[J]. *Frontiers in Bioengineering and Biotechnology*, 2019, 7: 135.

[3] WEI Z Y, ZHENG P P, CHEN Q K, et al. Correlation of corneal nerve innervation and ocular surface inflammationin in meibomain gland dysfunction [J]. *Chinese Journal of Ophthalmologic Medicine (Electronic Edition)*, 2021, 11(4): 205-210. (in Chinese)

[4] KANCLERZ P, KHORAMNIA R, WANG X G. Current developments in corneal topography and tomography[J]. *Diagnostics*, 2021, 11(8): 1466.

[5] KANDEL S, CHAUDHARY M, MISHRA S K, et al. Evaluation of corneal topography, pachymetry and higher order aberrations for detecting subclinical keratoconus[J]. *Ophthalmic and Physiological Optics*, 2022, 42(3): 594-608.

[6] SHEN Y, XIAN Y Y, HAN T, et al. Bilateral differential topography: a novel topographic algorithm for keratoconus and ectatic disease screening[J]. *Frontiers in Bioengineering and Biotechnology*, 2021, 9: 772982.

[7] DE ROJAS SILVA M V, TOBÍO RUIBAL A, SUANZES HERNÁNDEZ J. Corneal power measurements by ray tracing in eyes after small incision lenticule extraction for myopia with a combined Scheimpflug camera-Placido disk topographer[J]. *International Ophthalmology*, 2022, 42(3): 921-931.

[8] JIN Y L, MCALINDEN C, SUN Y, et al. Sirius Scheimpflug: Placido versus ultrasound pachymetry for central corneal thickness: meta-analysis[J]. *Eye and Vision*, 2021, 8(1): 5.

[9] XU D Y, GAO J X, SUI C H, et al. Image edge detection and shape reconstruction in corneal topography [J]. *Laser & Optoelectronics Progress*, 2017, 54(10): 209-214. (in Chinese)

[10] ZHOU H Y, SHEN J X, GAO S L, et al. Research and application of interpolation algorithm in corneal topography system[J]. *Manufacture Information Engineering of China*, 2011, 40(1): 54-56, 60. (in Chinese)

[11] FLORINDO J B, SOARES S H M, DE CARVALHO L A V, et al. Mumford-Shah algorithm applied to videokeratography image processing and consequences to refractive power values[J]. *Computer Methods and Programs in Biomedicine*, 2007, 87(1): 61-67.

[12] SUI C H, WO S J, XU D Y, et al. Design and implementation of Placido disk and projection lighting system for corneal topography [J]. *Optics and Precision Engineering*, 2017, 25(3): 603-610. (in Chinese)

[13] SONG L B, HE L B, HUO S J, et al. Comparison of refraction before and after pupil dilation in adolescents with initial myopia[J]. *China Glasses Science-Technology Magazine*, 2022(9):138-141. (in Chinese)

[14] ZHANG Z H, ZENG S, CAI J J, et al. Control effect of corneal plastic lens in children with myopia different diopters[J]. *Contemporary Medicine*, 2022, 28(13): 35-38. (in Chinese)

[15] YU Y C, JI X G, YAN C, et al. Research on multi-resolution fairing for non-uniform rational B-spline curves [J]. *Machine Design & Research*, 2019, 35(2): 1-5, 11. (in Chinese)

[16] ZHANG Y W. Research on B-spline fitting algorithm based on dense point cloud data[D]. Shanghai: Shanghai Institute of Technology, 2021. (in Chinese)

[17] WANG Z S, CHEN G L, WANG H, et al. A study on precision design of parallel mechanisms

based on mapping of error space[J]. *Machine Design & Research*, 2016, 32(4): 10-14. (in Chinese)
[18] JIANG S, JIANG W S. Reliable image matching via photometric and geometric constraints structured by Delaunay triangulation[J]. *ISPRS Journal of Photogrammetry and Remote Sensing*, 2019, 153: 1-20.
[19] MAFI M, MARTIN H, CABRERIZO M, et al. A comprehensive survey on impulse and Gaussian denoising filters for digital images[J]. *Signal Processing*, 2019, 157: 236-260.
[20] ZHOU H Y. Research on the reconstruction algorithms in corneal topography system and their applications [D]. Nanjing: Nanjing University of Aeronautics and Astronautics, 2010. (in Chinese)

基于 Placido 盘的角膜地形图成像

万晅润[1], 王超星[1], 胡 俊[2,3], 姜 俭[4,5*], 李康妹[1*]
1. 东华大学 机械工程学院, 上海 201620
2. 东华大学 人工智能研究院, 上海 201620
3. 上海市工业大数据工程技术研究中心, 上海 201620
4. 温州医科大学 眼科医院, 浙江 温州 325000
5. 浙江省眼科医院, 浙江 温州 325000

摘 要: 在眼科领域, 角膜地形图是进行诊断治疗的重要参考依据。复原度高的角膜地形图对临床实践有重要意义。该研究基于 Placido 盘采集到的角膜初始信息进行屈光度计算。以极坐标的方式建立角膜点云模型, 提出了一种在自定义插值矩阵中自寻控制点的方式下的局部双三次 B 样条缺失点填充插值算法。通过 Delaunay 三角剖分算法和高斯核函数平滑, 实现了点云信息的网格化插值和地形图平滑成像。试验表明, 该插值算法与之前算法相比具有更好的精度, 从最终成像的地形图得到的屈光度与检测得到的屈光度的平均误差在 0.300 D 以内。该算法具有较好的可行性。

关键词: 角膜地形图; Placido 盘; 点云模型; 双三次 B 样条; 高斯核函数